

Differential electrophysiological properties of dopamine D1 and D2 receptor-containing striatal medium-sized spiny neurons

Carlos Cepeda,* Véronique M. André,* Irene Yamazaki, Nanping Wu, Max Kleiman-Weiner and Michael S. Levine
Mental Retardation Research Center, David Geffen School of Medicine, NPI Room 58-258, 760 Westwood Plaza, University of California, Los Angeles, CA 90095, USA

Keywords: dopamine receptors, membrane properties, mouse, patch-clamp, striatum, synapses

Abstract

The electrophysiological properties of distinct subpopulations of striatal medium-sized spiny neurons (MSSNs) were compared using enhanced green fluorescent protein as a reporter gene for identification of neurons expressing dopamine D1 and D2 receptor subtypes in mice. Whole-cell patch-clamp recordings in slices revealed that passive membrane properties were similar in D1 and D2 cells. All MSSNs displayed hyperpolarized resting membrane potentials but the threshold for firing action potentials was lower in D2 than in D1 neurons. In voltage clamp, the frequency of spontaneous excitatory postsynaptic currents was higher in D2 than in D1 cells and large-amplitude inward currents (> 100 pA) were observed only in D2 cells. After tetrodotoxin this difference was reduced, suggesting that sodium conductances contribute to the increased frequencies in D2 cells. After pharmacological blockade of GABA_A receptors, a subset of D2 cells also displayed large spontaneous membrane depolarizations and complex responses to stimulation of the corticostriatal pathway. To further characterize ionotropic glutamate receptor function, α -amino-3-hydroxy-5-methyl-4-isoxazolepropionate (AMPA) was applied onto dissociated MSSNs. Application of AMPA alone or in the presence of cyclothiazide (an AMPA receptor desensitization blocker) evoked larger currents in D1 than in D2 cells. Together, these data demonstrate significant differences in electrophysiological properties of subpopulations of MSSNs defined by selective expression of D1 and D2 receptors. D2 cells display increased excitability and reflect ongoing cortical activity more faithfully than D1 cells, an effect that is independent of postsynaptic AMPA receptors and probably results from stronger synaptic coupling. This could help to explain the increased vulnerability of D2 MSSNs in neurodegenerative disorders.

Introduction

The ubiquitous medium-sized spiny neurons (MSSNs) comprise more than 90% of the striatal cell population (Kemp & Powell, 1971). Although all MSSNs are GABAergic, they differ in a number of properties including the expression of dopamine (DA) and acetylcholine receptor subtypes, peptide content, and their projection targets (Gerfen, 1992). Two neuronal subpopulations of MSSNs have been described, one that projects primarily to the substantia nigra pars reticulata and the internal segment of the globus pallidus (named the direct pathway), and another that projects primarily to the external segment of the globus pallidus (named the indirect pathway) (Smith *et al.*, 1998). MSSNs giving rise to the direct pathway mainly express DA D1 receptors and colocalize substance P, whereas MSSNs giving rise to the indirect pathway mainly express DA D2 receptors and colocalize enkephalin, although some overlap exists (Kawaguchi *et al.*, 1990; Surmeier *et al.*, 1996; Aizman *et al.*, 2000).

Examining the electrophysiological differences between these two cell populations may help in understanding their functions and differential vulnerability in neurodegenerative diseases involving the striatum. For example, considerable evidence indicates that cells

projecting to the external globus pallidus are more vulnerable in Huntington's disease (Albin *et al.*, 1992; Deng *et al.*, 2004). Previous attempts at defining differences in striatal cell subpopulations combined electrophysiological recordings with morphological methods (Kawaguchi *et al.*, 1989) or single-cell reverse transcriptase-polymerase chain reaction (Surmeier *et al.*, 1996; Venance & Glowinski, 2003). These methods have limitations as they can only define the fingerprint of a recorded cell *a posteriori*. Recently, mice that express enhanced green fluorescent protein (EGFP) reporter genes in a variety of cells have been generated (Gong *et al.*, 2003). In particular, mice that express specific DA and acetylcholine receptor subtypes represent an important tool to differentiate neuronal populations within the striatum. Two recent studies examined the electrophysiological properties and cortical inputs of D1 and D2 EGFP-positive MSSNs but the findings were inconsistent. In one study (Day *et al.*, 2006) no differences in cortical input were found, whereas in the other (Kreitzer & Malenka, 2007) marked differences were reported. A limitation in the first study was the age of the mice (17–25 days), as analyses were performed during a period of intense synaptic reorganization in the striatum (Uryu *et al.*, 1999), whereas in the second study muscarinic M4 EGFP-positive MSSNs were used as equivalent to D1 receptor-expressing cells, an assumption that may not be justified as a significant number of enkephalin-positive MSSNs also express M4 receptors (Bernard *et al.*, 1992).

Correspondence: Dr Michael S. Levine, as above.
E-mail: mlevine@mednet.ucla.edu

*C.C. and V.M.A. contributed equally to this work.

Received 30 August 2007, revised 19 November 2007, accepted 6 December 2007

We examined the basic membrane properties and spontaneous or evoked synaptic activity of D1 and D2 EGFP-positive MSSNs in striatal slices. In addition, α -amino-3-hydroxy-5-methyl-4-isoxazolepropionate (AMPA) receptor-mediated currents were examined in dissociated D1 and D2 cells. The data demonstrate both common and unique electrophysiological parameters for each subtype and support the hypothesis that these subpopulations of projection cells integrate different aspects of cortical information. A preliminary report of these studies was presented in abstract form at the Society for Neuroscience Meeting (Cepeda *et al.*, 2004).

Materials and methods

All experimental procedures were performed in accordance with the United States Public Health Service *Guide for Care and Use of Laboratory Animals* and were approved by the Institutional Animal Care and Use Committee at the University of California, Los Angeles. Experiments were conducted on D1 ($n = 17$ for slices and $n = 7$ for dissociated cells) and D2 ($n = 23$ for slices and $n = 9$ for dissociated cells) EGFP-positive mice older than 28 days (average 39.7 ± 1.6 days for slices and 45.8 ± 2.7 days for dissociated cells). In a series of initial experiments we also used muscarinic M4 EGFP-positive mice ($n = 4$, average 32 ± 2.9 days old) as a putative equivalent of D1 mice. Use of M4 mice was discontinued for reasons explained in the Results. Details of the methodology used to generate EGFP-positive mice have been published (Gong *et al.*, 2003) and are also available at the GENSAT web page (<http://www.gensat.org>). The colonies of the animals used in the present study were maintained at the University of California, Los Angeles. Mice were deeply anesthetized with halothane and decapitated.

Cell visualization and confirmation of cell identity

The EGFP-positive cells were visualized in slices or after acute dissociation using a 40 \times water immersion lens. The microscopes (BX50WI, Olympus, Center Valley, PA, USA or Axioskop, Zeiss, Thornwood, NY, USA) were equipped with Nomarski optics and fluorescence. For infrared (IR) videomicroscopy, a halogen lamp and an IR filter (790 nm, Ealing Optics, Holliston, MA, USA) were used. For fluorescence, labeled cells were excited with UV light. The light source consisted of a mercury lamp (100 W) and filtered light (450–480 nm) was detected with a video camera (QICAM-IR Fast 1394, Burnaby, BC, Canada) optimized to detect EGFP fluorescence and also able to detect IR light. Images were digitized and saved using the QCapture Pro software (version 5, Burnaby, BC, Canada). Once a viable medium-sized neuron in the slice was identified with IR videomicroscopy, the filter was switched to fluorescence mode to determine if it was also labeled with EGFP. The digitized IR image was superimposed over the fluorescence image and electrophysiological recordings proceeded only if the cell identified with IR light showed a complete overlap with EGFP fluorescence and was in the same focal plane.

Single-cell reverse transcriptase-polymerase chain reaction was performed on a subset of acutely dissociated MSSNs not used for recording to confirm expression of DA receptors, enkephalin and substance P. Only EGFP-positive cells from dorsal striatum were collected. All D1 EGFP-positive cells showed D1 receptor and substance P expression ($n = 14$), one (7%) also showed D2 receptor expression and none showed enkephalin expression. All D2 EGFP-positive cells expressed D2 receptor message ($n = 18$) and 83% (15/18) also expressed enkephalin. One (6%) also showed D1 receptor expression and three (17%) showed substance P expression.

Electrophysiological recordings in slices

Whole-cell patch-clamp recordings of D1 or D2 EGFP-positive MSSNs were obtained using standard methods (Cepeda *et al.*, 1998). Cells were also identified by somatic size, basic membrane properties (input resistance, membrane capacitance and time constant) and, in some cases, by addition of biocytin (0.2%) to the internal solution. The patch pipette (3–5 M Ω) contained one of the following solutions (in mM): (i) 140 K-gluconate, 10 N-[2-hydroxyethyl] piperazine-N-[2-ethanesulfonic acid] (HEPES), 2 MgCl₂, 0.1 CaCl₂, 1.1 ethylene glycol-bis (β -aminoethyl ether)-N,N,N',N'-tetra-acetic acid and 2 K₂ATP for voltage and current clamp or (ii) 130 Cs-methanesulfonate, 10 CsCl, 4 NaCl, 1 MgCl₂, 5 MgATP, 5 ethylene glycol-bis (β -aminoethyl ether)-N,N,N',N'-tetra-acetic acid, 10 HEPES, 0.5 GTP, 10 phosphocreatine and 0.1 leupeptin for voltage-clamp recordings (pH 7.25–7.3, osmolality, 280–290 mOsm). Access resistances were <25 M Ω . Spontaneous postsynaptic currents were recorded in standard artificial cerebrospinal fluid (ACSF) composed of the following (in mM): 130 NaCl, 26 NaHCO₃, 3 KCl, 2 MgCl₂, 1.25 NaHPO₄, 2 CaCl₂ and 10 glucose, pH 7.4 (osmolality, 300 mOsm). Cells were held at -70 mV to minimize the contribution of GABA_A receptors and voltage-gated conductances. In specific experiments, bicuculline (BIC) (20 μ M) or picrotoxin (50 μ M) was added to the external solution to abolish the activation of GABA_A receptors and to increase cortical synchronization (bursting activity). To isolate spontaneous excitatory postsynaptic currents (EPSCs) that were independent of action potential generation, tetrodotoxin (TTX) (1 μ M) was added to the external solution.

Passive membrane properties were determined in voltage-clamp mode by applying a depolarizing step voltage command (10 mV) and using the membrane test function integrated in the pClamp8 software (Axon Instruments, Foster City, CA, USA). This function reports membrane capacitance (in pF), input resistance (in M Ω or G Ω) and time constant (in μ s or ms). The time constant was obtained from a single exponential fit to the decay of the capacitive transients. After characterizing the basic membrane properties of the neuron, spontaneous EPSCs were recorded for 3–6 min. The membrane current was filtered at 1 kHz and digitized at 200 μ s using Clampex (Axon Instruments). Spontaneous EPSCs were analysed off-line using the Mini Analysis Program (Jaevin Software, Leonia, NJ, USA). The threshold amplitude for the detection of an event was adjusted above root mean square noise level (generally 2–3 pA). This software was used to calculate EPSC frequency and amplitude for each synaptic event, and to construct amplitude–frequency histograms. Frequencies were expressed as number of events per second (Hz). EPSC kinetic analysis used the Mini Analysis Program. Events with peak amplitudes between 5 and 50 pA were grouped, aligned by half-rise time and normalized by peak amplitude. Events with complex peaks were eliminated. In each cell, all events between 5 and 50 pA were averaged to obtain rise times, decay times and half-amplitude durations. First- and second-order exponential curves were fit with a maximum of 5000 iterations, and SDs between first- and second-order fits were compared.

In additional slices, evoked EPSCs were examined in normal ACSF and after the addition of BIC. For these experiments QX-314 (4 mM), a quaternary derivative of lidocaine that produces Na⁺ channel inactivation, was added to the internal Cs-methanesulfonate solution to block action potentials that could be induced at high stimulus intensities. EPSCs were evoked with a bipolar tungsten electrode, one lead in the deeper cortical layers and the other in the corpus callosum (~ 0.5 mm from the recording electrode). A series of current pulses of increasing intensity (0.1–1.6 mA, 0.5 ms pulse duration) were used to

determine evoked EPSC threshold and response amplitude at different stimulation intensities. A series of stimulus intensities (threshold, 2× and 3× threshold current) was used to compare response amplitudes, as well as the effects of BIC in cells from D1 and D2 EGFP animals. Three responses in ACSF and in BIC at each stimulus intensity were averaged and compared.

Acutely dissociated neurons

Slices from EGFP animals were also used for acute dissociation of neurons. After at least 1 h of incubation in the oxygenated ACSF, the dorsal striatum was dissected out of the coronal slices with the aid of a microscope. A striatal slice was placed in an oxygenated cell-stir chamber (Wheaton, Millville, NJ, USA) and enzymatically treated for 20 min with papain (0.5 mg/mL, Calbiochem) at 35 °C in a HEPES-buffered Hank's balanced salts solution (Sigma Chemical, St Louis, MO, USA) supplemented with (in mM): 1 pyruvic acid, 0.005 glutathione, 0.1 N^G-nitro-L-arginine and 1 kynurenic acid (pH 7.4, 300–310 mOsm). Striatal slices were then mechanically dissociated with a series of graded fire-polished Pasteur pipettes. The cell suspension was plated into a 35-mm nunclon Petri dish mounted on the stage of an upright fixed-stage microscope (Axioscope, Zeiss) containing a HEPES-buffered salt solution [containing (in mM): 140 NaCl, 23 glucose, 15 HEPES, 2 KCl, 2 MgCl₂ and 1 mM CaCl₂ (pH 7.4, 300–310 mOsm)].

Standard whole-cell patch-clamp techniques were used to obtain voltage-clamp recordings (Bargas *et al.*, 1994). Electrodes were pulled from Corning 8250 glass (A-M Systems, Carlsborg, WA, USA) and heat polished prior to use (3.5–5.5 MΩ). The internal solution consisted of (in mM): 175 N-methyl-D-glucamine, 40 HEPES, 2 MgCl₂, 10 ethylene glycol-bis (β-aminoethyl ether)-N,N,N',N'-tetraacetic acid, 12 phosphocreatine, 2 Na₂ ATP, 0.2 Na₂ GTP and 0.1 leupeptin (pH 7.25, 265–270 mOsm). The external solution consisted of (in mM): 135 NaCl, 20 CsCl, 3 BaCl₂, 2 CaCl₂, 10 glucose, 10 HEPES and 0.0003 TTX (pH 7.4, 300–310 mOsm). Cs⁺ and TTX were in the external solution to block some voltage-gated K⁺ and all Na⁺ channels, respectively.

Recordings were obtained with an Axon Instruments 200A patch-clamp amplifier and controlled by a computer running pClamp (v. 8.01) with a DigiData 1200 series interface (Axon Instruments). Negative pressure was carefully applied to obtain tight seals (> 1 GΩ). Additional negative pressure broke the membrane and created the whole-cell configuration. Data were collected from neurons that had access resistances < 20 MΩ. There were no significant differences between mean access resistances among groups. After whole-cell configuration was reached, series resistance was compensated (70–90%) and periodically monitored. All recordings were made from medium-sized neurons. After obtaining basic membrane properties, currents induced by AMPA alone or in the presence of 10 μM cyclothiazide (CTZ) (a drug that prevents AMPA receptor desensitization) were examined by applying 100 μM of the agonist (3 s every 20 s) while holding the cell at –80 mV. Drugs were applied with a pressure-driven fast perfusion system through capillaries positioned a few hundred micrometers from the cell. A DC drive system controlled by an SF-77B perfusion system (Warner Instruments, Hamden, CT, USA) synchronized by pClamp changed solutions by moving the position of the capillaries. Values for peak currents and peak current densities were calculated for all neurons. Current density was obtained by dividing currents by cell capacitance to normalize values with respect to cell size (Alzheimer *et al.*, 1993).

Statistics

Values in the figures and text are presented as means ± SEM. Differences in mean values were assessed with Student's *t*-tests (two groups) or appropriate ANOVAS (multiple groups) followed by multiple comparisons using Bonferroni *t*-tests. When comparing the proportion of cells showing an effect, Fisher exact tests were used. Differences between means were considered statistically significant if *P* < 0.05.

Results

Basic membrane properties of MSSNs in slices

Based on their typical electrophysiological membrane properties and the morphology of biocytin-labeled neurons, only MSSNs were recorded. Figure 1A shows examples of a D1 and a D2 EGFP-positive neuron after biocytin processing. The passive membrane properties of D1 or D2 EGFP-positive cells in slices were determined in voltage-clamp mode using a small depolarizing step voltage command (10 mV) from a holding potential of –70 mV. Because the measurements of these properties were not significantly different regardless of the internal solution in the patch pipette, data were pooled for the two internal solutions. There were no significant differences in cell capacitance (70.1 ± 3.3 and 72.4 ± 2.2 pF), input resistance (186.7 ± 19.9 and 181.2 ± 15.3 MΩ) or time constant (1.6 ± 0.1 and 1.5 ± 0.1 ms) between D1 (*n* = 40) and D2 (*n* = 65) cells, respectively. After assessment of passive membrane properties, recordings were switched to current-clamp mode (K-gluconate in the patch pipette). All MSSNs displayed hyperpolarized resting membrane potentials (–82.1 ± 1.4 mV in D1 and –82.2 ± 1.2 mV in D2 cells). Injection of hyperpolarizing and depolarizing current pulses showed that both groups of cells displayed inward rectification, a typical feature of MSSNs (Fig. 1B, Cepeda *et al.*, 1994). Examination of action potentials evoked with depolarizing current pulses or with continuous current injection did not reveal significant differences in amplitude, half-amplitude duration or afterhyperpolarization amplitudes between D1 and D2 cells (Fig. 1C). However, the threshold membrane potential for inducing action potentials was more depolarized in D1 than in D2 neurons (–48.4 ± 1.5 and –53.0 ± 1.3 mV, respectively, *P* < 0.03), indicating that D2 cells were more excitable (Fig. 1C).

Spontaneous synaptic currents

Spontaneous inward currents were recorded in voltage-clamp mode at a holding potential of –70 mV in regular ACSF. At this holding potential spontaneous inward currents are mediated by non-N-methyl-D-aspartate ionotropic glutamate receptors as 6-cyano-7-nitroquinoline-2,3-dione (10 μM) completely abolishes spontaneous EPSCs (Cepeda *et al.*, 2003). Average frequencies were significantly higher in D2 than in D1 cells (2.9 ± 0.2 and 1.8 ± 0.2 Hz, respectively, *P* < 0.001, *n* = 59 D2 and *n* = 34 D1 cells, Fig. 2A and B). Initially we had collapsed the data from D1 and M4 cells assuming that, based on receptor localization, they would be equivalent. However, we soon realized that the frequency of spontaneous EPSCs recorded in M4 EGFP-positive cells (3.1 ± 0.4 Hz, *n* = 11, Fig. 2B inset) was different from the frequency in D1 cells and was closer to the frequency in D2 cells, suggesting that the overlap of D1 and M4 receptors may not be absolute. For that reason, we decided not to use data from M4 cells in this comparative study.

The higher spontaneous EPSC frequency in D2 compared with D1 cells occurred across virtually all amplitude bins and pairwise

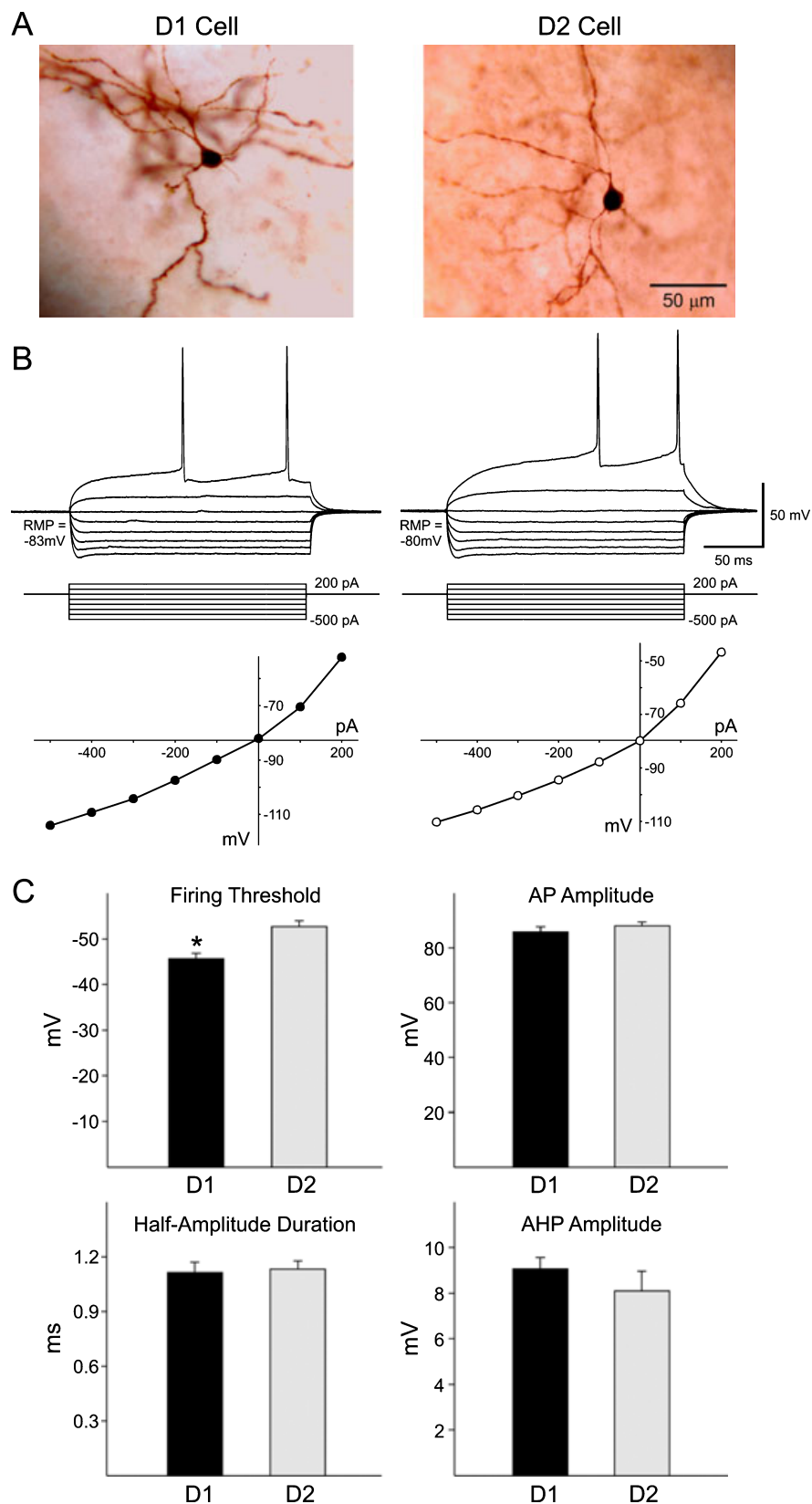


FIG. 1. (A) D1 and D2 EGFP-positive cells visualized with infrared videomicroscopy and differential interface contrast optics and recorded with a patch electrode and subsequently processed for biocytin. Calibration applies to both panels. (B) Voltage changes produced by injection of hyperpolarizing and depolarizing current pulses (100 pA steps) and current–voltage plots generated by measuring the voltage change as a function of current intensity. Note the presence of inward rectification, a typical feature of MSSNs. (C) Bar graphs show the action potential characteristics as well as the voltage threshold to induce action potentials. The threshold was significantly more depolarized in D1 than in D2 neurons, indicating that D1 cells require more depolarizing current to generate action potentials. *Mean values were significantly different. RMP, resting membrane potential; AP, action potential; AHP, after-hyperpolarisation.

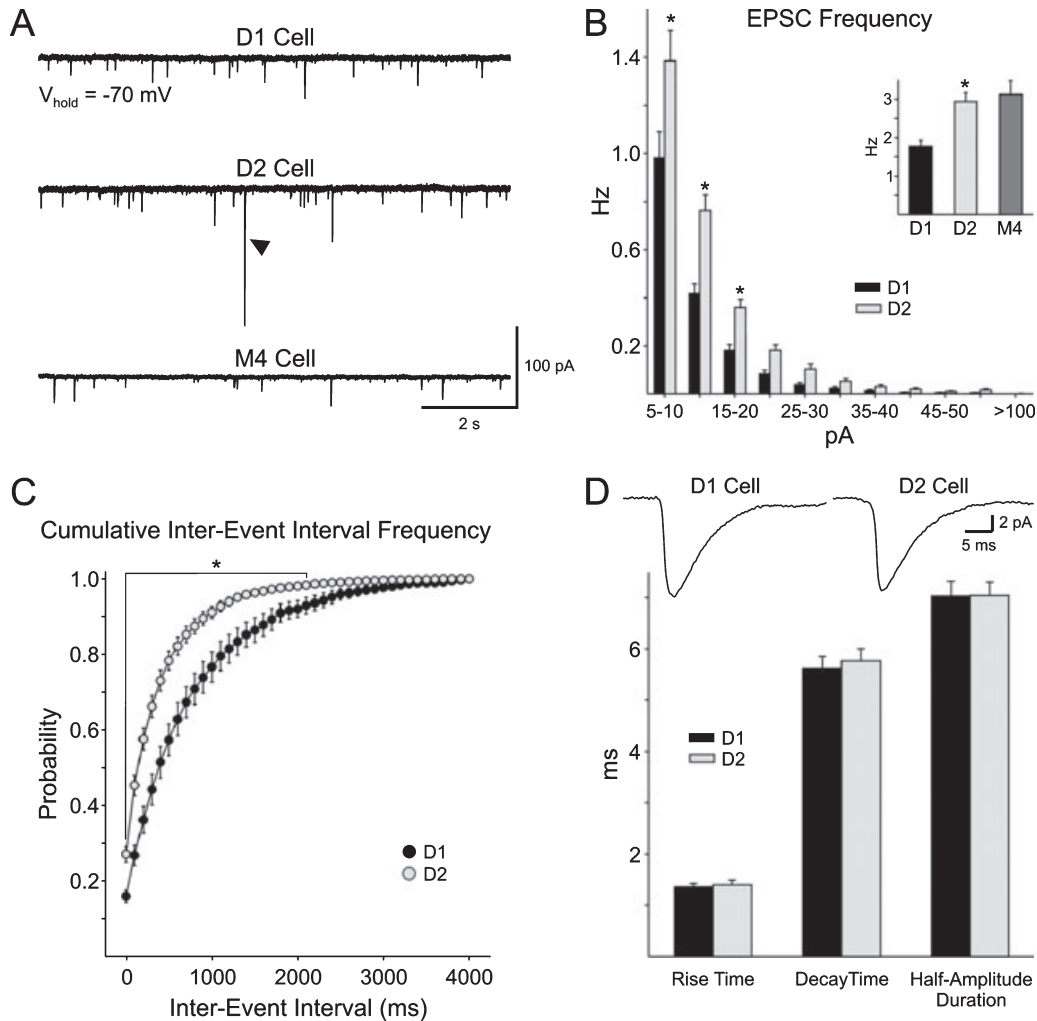


FIG. 2. Spontaneous synaptic currents in D1 and D2 EGFP-positive MSSNs. (A) Examples of spontaneous synaptic currents recorded in voltage-clamp mode in a D1, a D2 and a M4 cell while holding the membrane at -70 mV. Notice the occurrence of a very large synaptic event (arrowhead) in the D2 cell. (B) Amplitude–frequency histograms showed that the frequency of synaptic currents was greater in D2 than in D1 cells across amplitude bins. Inset shows the average frequency of spontaneous synaptic currents in D1 and D2 cells. The difference between mean frequencies of D1 and D2 cells was statistically significant. For comparison, the average frequency of spontaneous synaptic currents in M4 cells is also illustrated. (C) Cumulative interevent interval distributions in D1 and D2 cells show that there are significantly more shorter intervals in D2 cells, indicating increased release probability. Bracket shows the differences between mean values for bins that were statistically significant. (D) Traces are averages of spontaneous synaptic currents (5–50 pA) recorded in a D1 and a D2 cell. Kinetic properties were similar in both subpopulations of cells. *Mean values were significantly different.

multiple comparisons showed that the difference in frequency of small-amplitude events (5–20 pA, 5 pA bins) was statistically significant ($P < 0.001$, Bonferroni t -test). Individual bins for larger-amplitude events (> 20 pA) were not significantly different but, when grouped together (20–100 pA), the difference in frequency was highly significant (0.43 ± 0.02 Hz in D2 and 0.18 ± 0.03 Hz in D1 cells, $P < 0.001$). In addition, spontaneous synaptic currents > 100 pA were seen in 5 of 59 D2 and 0 of 34 D1 cells ($P = 0.029$, Fisher exact test on the numbers of cells per group showing events > 100 pA). Finally, cumulative interevent interval distributions demonstrated that D2 cells displayed proportionately more shorter intervals than D1 cells (Fig. 2C), indicating that corticostriatal terminals making synapses onto D2 cells have a higher probability of release than those making contact with D1 cells. In contrast, average amplitudes of events between 5 and 50 pA were similar in D1 and D2 cells (11.1 ± 0.5 and 11.4 ± 0.5 pA, respectively). Cumulative amplitude distributions were also essentially identical (data not shown). The kinetic properties of spontaneous

EPSCs were examined by comparing the average waveforms of all synaptic events between 5 and 50 pA from D1 and D2 MSSNs ($n = 38$ D1 and $n = 48$ D2 cells). Event rise and decay times, and half-amplitude durations of EPSCs were similar in D1 and D2 cells (Fig. 2D).

In a subset of MSSNs ($n = 13$ D1 and $n = 14$ D2 cells) TTX ($1 \mu\text{M}$) and BIC ($10 \mu\text{M}$) were added to the ACSF to isolate spontaneous, action potential-independent, miniature EPSCs (mEPSCs). The mean frequency of mEPSCs was slightly higher in D2 than in D1 cells but the difference was not statistically significant (Fig. 3A and B). Similarly, pairwise comparisons of amplitude–frequency bins did not yield statistical significance. Cumulative interevent interval distributions showed significant differences in a smaller number of interval bins (Fig. 3C) than occurred with spontaneous EPSCs (Fig. 2C). The reduced difference in cumulative distributions in the presence of TTX indicates that action potentials generated by cortical pyramidal neurons contributed to the increase in frequency observed in D2 cells, a suggestion corroborated by the fact

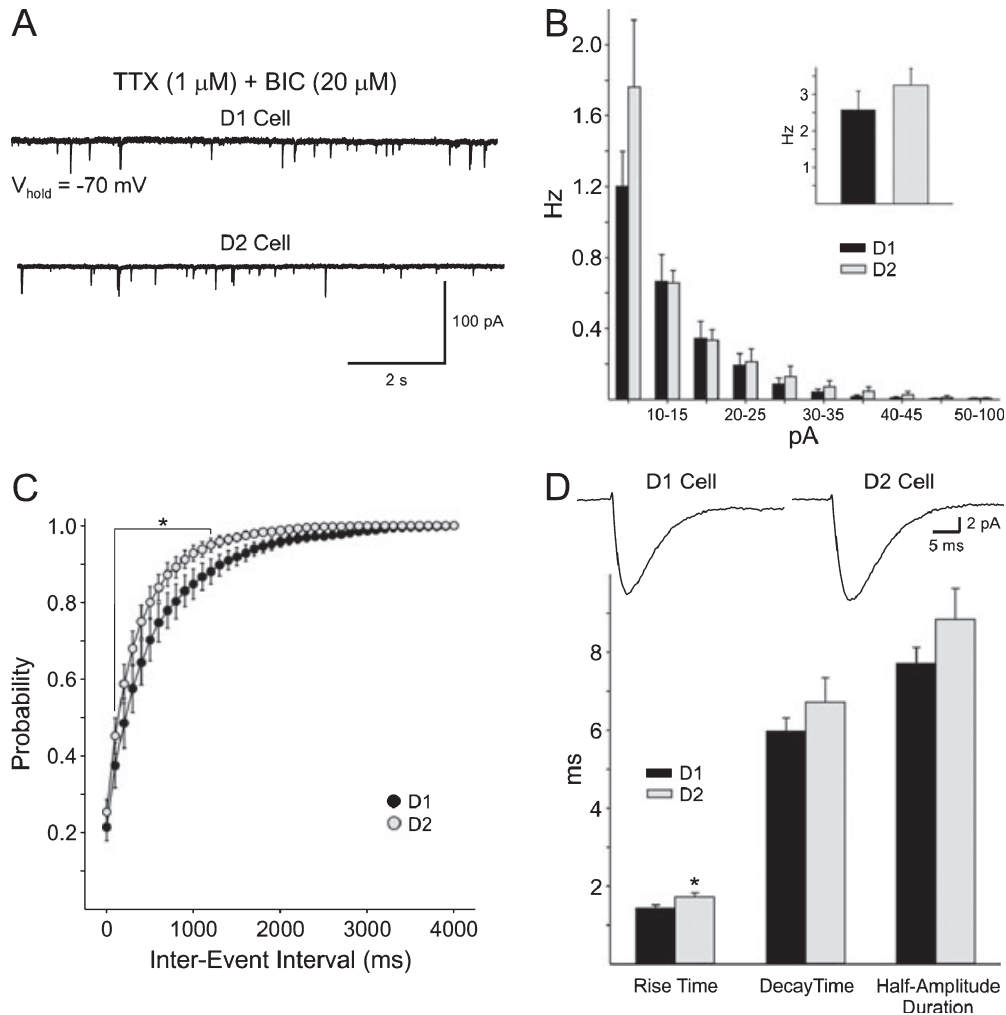


FIG. 3. Spontaneous mEPSCs in D1 and D2 EGFP-positive MSSNs in the presence of TTX and BIC. (A) Examples of mEPSCs recorded in voltage-clamp mode in D1 and D2 cells while holding the membrane at -70 mV. (B) Amplitude–frequency histograms showed that the frequencies of mEPSCs were similar in both cell groups across amplitude bins. Inset shows the average frequency of mEPSCs in D1 and D2 cells. (C) Interevent interval distributions of mEPSCs in D1 and D2 cells show that, in the presence of TTX and BIC, D2 cells still have more shorter intervals but in fewer bins than in normal ACSF (Fig. 2C). Bracket shows the differences between mean values for bins that were statistically significant. (D) Traces are averages of mEPSCs (5 – 50 pA) recorded in a D1 and a D2 cell. Kinetic properties were similar in both cell groups, except that the rise time was significantly longer in D2 cells. *Mean values were significantly different.

that very large amplitude events (i.e. those dependent on action potentials) only occurred in D2 cells.

The average amplitude of mEPSCs (9.7 ± 0.7 pA in D1 and 10.3 ± 1.1 pA in D2 cells) and the cumulative amplitude distributions were similar in D1 and D2 cells. The kinetic properties of spontaneous mEPSCs were examined by comparing the average waveforms of all synaptic events between 5 and 50 pA from D1 and D2 EGFP-positive MSSNs. Decay times and half-amplitude durations of mEPSCs were similar in D1 and D2 cells. In contrast, the rise times of events from D2 cells were significantly longer than those from D1 cells (Fig. 3D). The decay phase of the mEPSCs was well-fit by a first-order exponential curve.

Effects of GABA_A receptor blockade on spontaneous synaptic activity

As the previous observations suggested increased spontaneous, TTX-sensitive release of glutamate at the corticostriatal synapse in D2 cells, we next examined the effects of blockade of GABA_A receptors,

known to induce cortical synchronization, bursting and epileptiform activity (Gutnick *et al.*, 1982). This epileptiform activity may propagate to the striatum and produce membrane depolarizations with or without action potentials (Cepeda *et al.*, 2001; Bracci *et al.*, 2004). When slices from D1 or D2 mice were bathed in BIC (20 μ M) or picrotoxin (50 μ M), about one half of D2 EGFP-positive cells (6 out of 11) displayed large, long-lasting spontaneous membrane depolarizations in current clamp (Fig. 4A) and inward currents in voltage clamp (not shown), probably associated with bursting activity in the cerebral cortex. These depolarizations were rarely seen in D1 cells (1 out of 10). The probability of occurrence of these depolarizations was significantly higher in D2 compared with D1 cells ($P = 0.024$, Fisher exact test).

Evoked synaptic currents and effects of GABA_A receptor blockade

Electrical stimulation of the cortex and corpus callosum was used to further examine possible differences in cortical excitatory inputs into

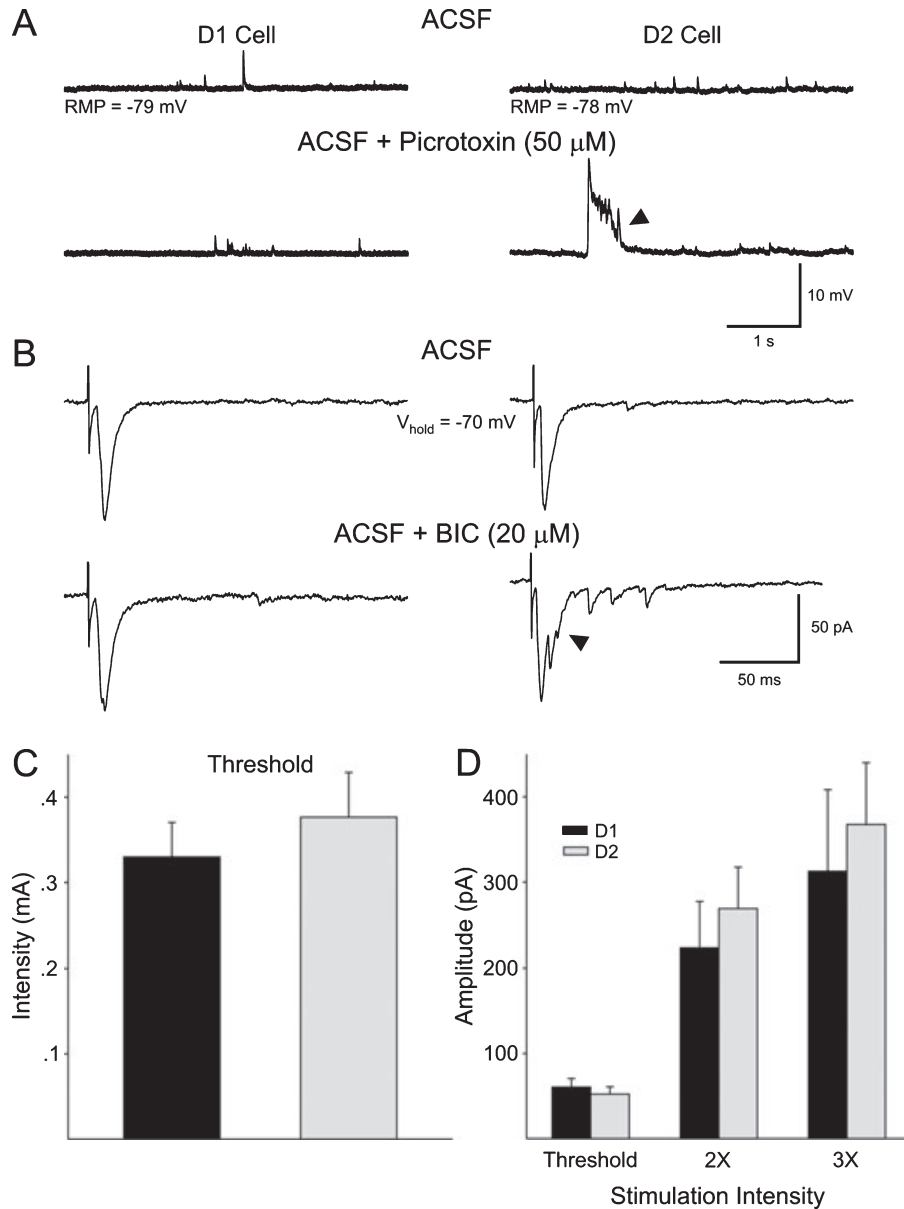


FIG. 4. (A) Effects of GABA_A receptor blockade. Examples of current-clamp recordings before and after bath application of picrotoxin in a D1 and a D2 cell. After blockade of GABA_A receptors the D2 EGFP-positive cell displayed large, long-lasting membrane depolarizations (arrowhead). (B) Evoked synaptic currents in D1 and D2 EGFP-positive MSSNs. Stimulation of the cortex and corpus callosum induced inward currents in D1 and D2 cells. After application of BIC, a subset of D2 cells displayed complex, long-lasting responses (arrowhead). (C) Bar graph shows that the threshold current required to induce EPSCs is similar in D1 and D2 cells. (D) Average response amplitudes at a series of increasing stimulation intensities. Amplitudes were similar in D1 and D2 cells. RMP, resting membrane potential.

D1 and D2 cells. Although the mean threshold current to evoke an EPSC was similar in both groups (0.38 ± 0.05 mA, $n = 17$ D1 and 0.33 ± 0.04 mA, $n = 20$ D2 cells), the proportion of D2 cells that responded to lower stimulation intensities (less than the mean threshold) was significantly higher than that of D1 cells (75 and 59%, respectively, $P < 0.001$, Fisher exact test), supporting the hypothesis that cortical activation is more likely to propagate to D2 cells. The average EPSC peak amplitudes in D1 and D2 cells were similar at each stimulation intensity (1×, 2× and 3× threshold intensity, Fig. 4C and D). However, D2 cells tended to display larger EPSC areas than D1 cells. This difference was due to slower rise and decay times and increased half-amplitude durations. Rise time and half-amplitude durations were significantly longer in D2 cells at 1× stimulation intensity (2.6 ± 0.3 and 4.1 ± 0.5 ms for rise time,

$P < 0.01$, and 7.2 ± 0.7 and 9.7 ± 0.9 ms for half-amplitude duration, $P < 0.03$, in D1 and D2 cells, respectively). Bath application of BIC uncovered additional differences between D1 and D2 cells. In 4 out of 20 D2 cells BIC ($20 \mu\text{M}$) induced an increase in the duration and complexity of the evoked EPSCs (Fig. 4B arrowhead). These responses were reminiscent of the spontaneous epileptiform discharges occurring after bath application of BIC and could also reflect cortical synchronization and bursting. These complex EPSCs were never observed in D1 EGFP-positive cells.

To examine possible differences in short-term synaptic plasticity between D1 and D2 cells, paired-pulse ratios (PPRs) of evoked EPSCs were examined at two stimulus intervals (50 and 100 ms) (Fig. 5A and B). The PPRs were similar at 50 ms stimulus intervals in D1 and D2 cells (1.2 ± 0.1 in D1 and 1.3 ± 0.1 in D2 cells, $n = 12$ and $n = 13$,

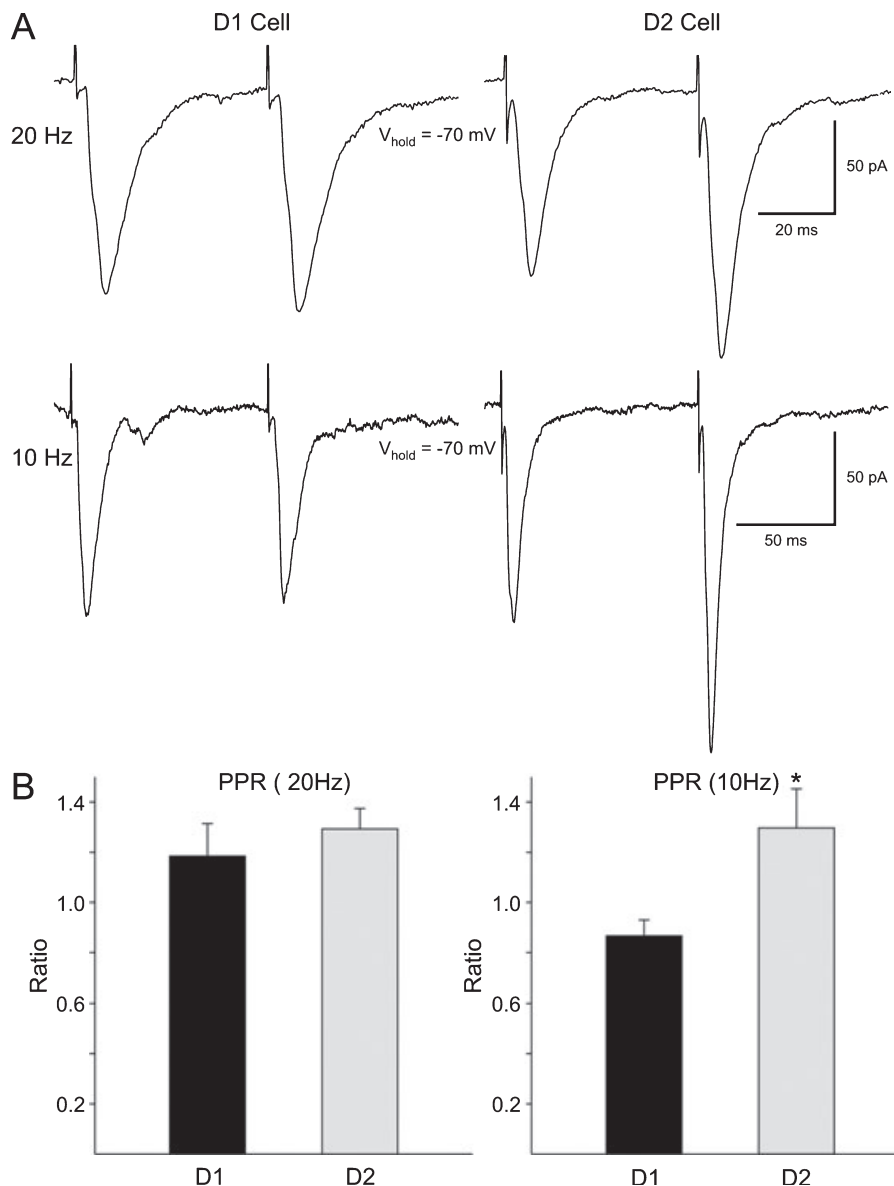


FIG. 5. (A) EPSCs induced by paired-pulse stimulation at two interstimulus intervals [50 ms (20 Hz, top) and 100 ms (10 Hz, bottom)] in D1 and D2 cells. Traces represent the average of three consecutive stimulations 30 s apart. (B) Graphs indicate the average PPR in D1 and D2 cells at both interstimulus intervals. At 50 ms the PPRs were similar in D1 and D2 cells. At 100 ms there was a significant difference in PPRs, with D2 cells displaying higher PPR. *Mean values were significantly different.

respectively). However, the percentage of D2 cells (85%) showing paired-pulse facilitation (PPF) was larger than the percentage of D1 cells (50%). At 100 ms intervals the PPR was significantly larger in D2 than in D1 cells (1.3 ± 0.2 and 0.9 ± 0.1 , respectively; $P = 0.03$). Similarly, the percentage of D2 cells (62%) showing PPF was larger than the percentage of D1 cells (27%).

Passive and active membrane properties of dissociated MSSNs

In dissociated MSSNs ($n = 27$ D1 and $n = 45$ D2 cells), mean cell capacitances were significantly greater in D1 than in D2 cells (13.4 ± 0.3 and 12.2 ± 0.2 pF, respectively, $P < 0.05$). In contrast, mean input resistances (2.0 ± 0.2 and 2.2 ± 0.2 G Ω) and mean time constants (151.4 ± 14.1 and 137.3 ± 8.1 μ s) were similar. Voltage-gated Ca^{2+} currents were also examined. Peak currents and current

densities evoked by depolarizing step voltage commands (from -80 to -10 mV) were similar in D1 and D2 cells (219 ± 32 vs. 173 ± 17 pA for peak currents and 17.0 ± 2.4 vs. 16.0 ± 1.1 pA/pF for current densities, respectively).

Responses to AMPA in dissociated MSSNs

AMPA (100 μ M) induced a fast desensitizing current that was followed by a steady-state current in D1 ($n = 27$) and D2 ($n = 45$) cells (Fig. 6A, left two traces). AMPA peak current densities were significantly larger in D1 compared with D2 cells ($P = 0.048$, Fig. 6B). Steady-state current amplitudes and densities were significantly larger in D1 compared with D2 cells ($P = 0.02$ for current amplitude and $P = 0.01$ for current density). Peak : steady-state ratios were significantly smaller in D1 (1.8 ± 0.1) than in D2 (2.1 ± 0.1)

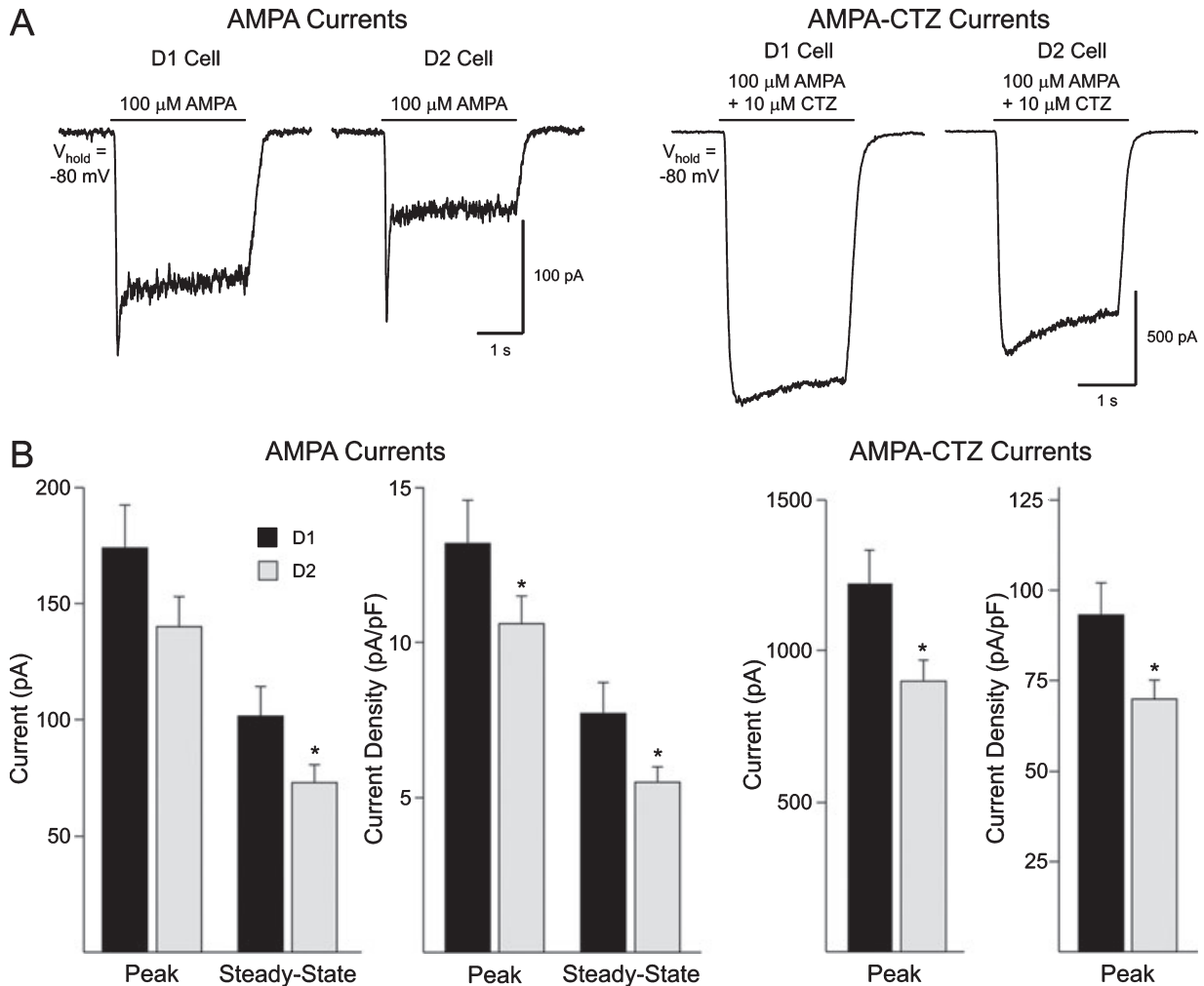


FIG. 6. (A) Traces show currents induced by AMPA (100 μ M) alone or in the presence of CTZ (10 μ M) in a D1 and a D2 cell. (B) Bar graphs show that peak amplitudes and densities for AMPA and AMPA-CTZ currents were larger in D1 cells. Steady-state amplitudes and densities for AMPA currents were also larger in D1 cells. *Mean values were significantly different.

cells ($P = 0.048$), indicating less receptor desensitization in D1 cells. Due to the fact that AMPA currents desensitize rapidly and the accurate measurement of the peak can be a concern if the application system is not rapid enough, AMPA currents were also examined in the presence of CTZ, an inhibitor of AMPA receptor desensitization. CTZ (10 μ M) increased AMPA currents by about sevenfold in both D1 and D2 cells (Fig. 6A, right traces). AMPA-CTZ peak current amplitudes and densities were also significantly larger in D1 compared with D2 cells ($P = 0.002$ for current amplitude and $P = 0.004$ for current density, Fig. 6B, right graphs).

Discussion

The present results demonstrate that D1 and D2 MSSNs both share common electrophysiological properties and display unique and significant differences that include (in slices): a reduced threshold to induce action potentials and increased frequency of spontaneous, TTX-sensitive synaptic currents in D2 cells, the occurrence of spontaneous, large-amplitude synaptic events and large membrane depolarizations after blockade of GABA_A receptors in D2 cells, and (in dissociated cells) larger AMPA currents in D1 cells. These findings further our knowledge of the distinct roles of these two subpopulations

and their association with the direct and indirect striatal output pathways. There are some caveats that need to be considered when associating D1 and D2 DA receptor-expressing neurons with each of these pathways. For example, it is well known that a percentage of these neurons can express both D1 and D2 receptors (Kawaguchi *et al.*, 1990; Surmeier *et al.*, 1996; Aizman *et al.*, 2000) and/or give rise to axon collaterals projecting to both pathways (Levesque & Parent, 2005).

Passive and active membrane properties

Passive membrane properties of D1 and D2 cells were similar in slices. In contrast, dissociated D2 EGFP-positive MSSNs had a smaller capacitance than D1 cells. In slices, the dendritic tree and spines account for most of the cell capacitance measured, whereas in dissociated neurons most of these processes are lost, which could partially explain the discrepancy between dissociated and slice preparations. Alternatively, space-clamp limitations in slices may preclude accurate measurement of cell membrane capacitance. In slice recordings, action potential properties were similar in D1 and D2 cells. However, D2 cells could produce action potentials from more hyperpolarized membrane potentials, indicating that they are more

readily available to transfer information than D1 cells. Increased firing rates after injection of depolarizing current pulses in D2 EGFP-positive cells were reported by Kreitzer & Malenka (2007) but differences in firing threshold or rheobase were not examined. Based on the present results, the increased excitability of D2 cells is due to a lower firing threshold. It is unlikely that this increased excitability was due to changes in input resistance or afterhyperpolarization amplitude, as these parameters were similar in D1 and D2 cells in slices. However, a recent study reported differences in Kir2 potassium channel subunit composition in D1 and D2 cells (Shen *et al.*, 2007). More studies are needed to determine possible changes in voltage-gated sodium and potassium conductances in D1 and D2 cells.

Synaptic inputs

In normal ACSF, D2 cells displayed higher frequencies of spontaneous synaptic inward currents when compared with D1 cells. Increased frequency of synaptic currents could indicate more inputs and glutamate release onto D2 cells. The difference in frequency was diminished after addition of TTX, indicating that the increase in frequency of spontaneous EPSCs in D2 cells is partially dependent on action potential generation. Previous studies examining spontaneous mEPSCs have yielded contrasting results. Whereas one study (Day *et al.*, 2006) did not find differences the other (Kreitzer & Malenka, 2007) demonstrated significant differences in frequency. As we pointed out, failure to find differences could have been due to the young age of the mice (17–25 days), a period when intense synapse formation and elimination occurs, particularly in the dorsolateral striatum (Uryu *et al.*, 1999). The other study used M4 instead of D1 EGFP mice and assumed equivalence of the two types of cells. However, the issue of D1 and M4 colocalization in MSSNs remains unresolved and the degree of overlap is not absolute (Bernard *et al.*, 1992). It is thus possible that M4 and D1 cells differ in terms of intrinsic properties and cortical inputs. Results from our laboratory indicate that M4 and D1 cells may have different electrophysiological properties, including differences in spontaneous synaptic currents.

In normal ACSF, D2 cells also displayed large-amplitude synaptic events (> 100 pA) never seen in D1 cells. These events are usually dependent on the occurrence of action potentials in the presynaptic neuron and could indicate that D1 and D2 MSSNs differ in the type of synaptic inputs that they receive. However, they could also be due to an increased number of glutamate receptors at the postsynaptic density. Based on data from dissociated MSSNs this appears unlikely because AMPA currents were smaller in D2 than in D1 cells. One possibility is that the synaptic surface area is larger in D2 cells. Morphological studies have shown that the size of corticostriatal terminals making synaptic contacts with D2-immunolabeled spines is significantly larger than those making contact with D1-immunolabeled spines (Lei *et al.*, 2004). A possible functional consequence of this differential innervation could be that D2 cells are subject to increased action potential-dependent glutamate release from corticostriatal terminals. Interestingly, cortical pyramidal neurons innervating the indirect pathway (probably D2 cells) also receive more excitatory inputs due to enlarged dendritic trees in layer I compared with pyramidal neurons innervating the direct pathway (probably D1 cells) (Morishima & Kawaguchi, 2006).

Electrical stimulation of the corticostriatal pathway evoked EPSCs at lower intensities in D2 than in D1 cells. Also, the response area tended to be larger and the kinetics slower in D2 compared with D1 cells, consistent with the idea that cortical inputs have a greater impact on D2 than in D1 cells. Average PPR at 50 ms intervals was

similar in D1 and D2 cells, and both displayed PPF or depression. At 100 ms intervals the PPR was higher in D2 than in D1 cells and at both interstimulus intervals more D2 cells displayed PPF. This finding indicates that, based on PPRs, it is very difficult to distinguish D1 and D2 cells as both can display PPF or depression. However, the fact that more D2 cells display PPF suggests differences in short-term synaptic plasticity between the two groups. In contrast, it was reported that D2 cells had lower PPR compared with M4- or D2-negative cells (Kreitzer & Malenka, 2007). Methodological differences, such as stimulation sites, could partially account for this discrepancy.

Increased PPR has been interpreted traditionally as reflecting low probability of release. In the present study this was not the case as, based on spontaneous synaptic release, D2 cells had higher, not lower, release probability. Numerous factors are involved in short-term synaptic changes such as, among others, the size of the releasable pool of synaptic vesicles (Saviane *et al.*, 2002) as well as regional differences in striatum (Smith *et al.*, 2001). Also, it has been suggested that spontaneously recycling vesicles and activity-dependent recycling vesicles originate from distinct pools (Sara *et al.*, 2005). It could be speculated that terminals impinging upon D2 cells are endowed with an increased number of releasable vesicles, consistent with anatomical evidence for larger excitatory synaptic contacts onto these cells (Lei *et al.*, 2004).

The idea that D2 cells receive more action potential-dependent glutamatergic inputs is reinforced by the observation that application of GABA_A receptor antagonists induced large-amplitude membrane depolarizations preferentially in D2 cells. These depolarizations reflect increased cortical synchronization typically produced by blockade of GABA_A receptors. The preferential propagation of epileptiform activity onto D2 cells thus confirms a tighter synaptic coupling between cortical pyramidal neurons and this particular subpopulation of MSSNs, in support of previous data demonstrating that enkephalin-positive neurons are selectively activated by cortical stimulation (Berretta *et al.*, 1997).

Glutamate receptors

Inward currents evoked by AMPA alone or in the presence of CTZ were larger in D1 cells. This finding was unexpected as we would have predicted AMPA currents to be larger in D2 cells, based on the presence of large spontaneous synaptic AMPA currents in slices. However, as indicated above, larger synaptic currents are probably based on action potentials and/or larger corticostriatal synapse areas. Further, in dissociated preparations the glutamate agonist activates both synaptic and extrasynaptic receptors, and more somatic than dendritic receptors. The reason why AMPA currents are smaller in D2 cells could be because there are fewer receptors, as indicated by the decreased current densities, but also because AMPA receptors have different subunit composition (Deng *et al.*, 2007). AMPA receptor mRNA editing at the R/G site, subunit composition (GluR1–4) and splice variants ('flip' and 'flop') determine the current amplitude and kinetics (Burnashev *et al.*, 1992; Geiger *et al.*, 1995; Partin *et al.*, 1996; Brorson *et al.*, 2004) and could also be different in D1 and D2 cells (Tallaksen-Greene & Albin, 1996; Vorobjev *et al.*, 2000).

Functional considerations

The present findings provide information relevant for both normal physiological function and dysfunction of particular MSSNs in

neurological diseases. The results could help to explain the observation that in Huntington's disease the striatal projection to the external pallidal segment (indirect pathway) is the most vulnerable (Deng *et al.*, 2004). One of the earliest morphological changes in Huntington's disease is the reduction in enkephalin expression, which is expressed primarily in neurons of the indirect pathway (Reiner *et al.*, 1988; Sapp *et al.*, 1995; Menalled *et al.*, 2000). It has been suggested that a critical determinant of the vulnerability of MSSNs is the extent to which they receive input from cortical or any other huntingtin-rich glutamatergic neurons (Fusco *et al.*, 1999). Our electrophysiological studies in genetic mouse models of Huntington's disease, such as the R6/2, have demonstrated a transient increase (around 5–7 weeks) in the frequency of large synaptic events in a subset of MSSNs followed by a progressive reduction of cortical inputs into the striatum (Cepeda *et al.*, 2003). It is tempting to speculate that the transient surge occurs primarily on the D2, enkephalin-expressing neurons, because these neurons have greater cortical synaptic inputs and are more directly affected by cortical activity as we have shown here. Thus, these D2-expressing neurons would be more vulnerable to dysfunction in the corticostriatal pathway (Cepeda *et al.*, 2007).

The present findings may provide additional alternative explanations for recent data suggesting that loss of spines in models of Parkinson's disease selectively affects D2 EGFP-positive MSSNs (Day *et al.*, 2006). Although strong evidence was presented that this effect could be attributed to dysregulation of postsynaptic L-type channels, it is possible that there is a presynaptic contribution. DA-depleting lesions have been shown to increase spontaneous glutamate-mediated synaptic activity in current-clamp (Galarraga *et al.*, 1987; Cepeda *et al.*, 1989; Calabresi *et al.*, 1993) and voltage-clamp (Gubellini *et al.*, 2002; Day *et al.*, 2006) recordings using high K⁺ in the patch electrode, conditions that more closely mimic a physiological situation. DA depletion also increases cell firing in striatopallidal neurons (Mallet *et al.*, 2006), decreases the threshold to evoke cortical responses (Florio *et al.*, 1993) and facilitates the flow of cortical membrane oscillations in a subpopulation of striatal neurons (Tseng *et al.*, 2001). Although these alterations can be attributed to changes in membrane potential or input resistance, postsynaptic changes may not be primary but secondary to dysregulation of glutamate release (Cepeda *et al.*, 2001).

Conclusions

In conclusion, the use of genetically modified mice expressing EGFP in specific striatal neuronal populations reveals electrophysiological differences between D1 and D2 cells. There are subtle changes in membrane properties likely to affect synaptic integration and these subpopulations differ in the nature of their cortical inputs. Thus, compared with D1 cells, D2 cells appear to reflect more faithfully the on-going cortical activity (cf. Mink, 1996), particularly the activity generated by pyramidal tract-type cortical neurons that preferentially innervate D2 cells (Lei *et al.*, 2004). Understanding the informational content and value of different cortical inputs and the way that different subpopulations of MSSNs process those inputs will further our knowledge of striatal functions in physiological and pathological states.

Acknowledgements

The authors want to acknowledge Drs Nat Heinz (GENSAT) and William Yang (UCLA) for supplying the EGFP-positive mice. We also thank Donna Crandall for help with the illustrations. Supported by USPHS Grant NS33538.

Abbreviations

ACSF, artificial cerebrospinal fluid; AMPA, α -amino-3-hydroxy-5-methyl-4-isoxazolepropionic acid; BIC, bicuculline; CTZ, cyclothiazide; DA, dopamine; EGFP, enhanced green fluorescent protein; EPSC, excitatory postsynaptic current; HEPEs, N-[2-hydroxyethyl] piperazine-N-[2-ethanesulfonic acid]; IR, infrared; mEPSC, miniature excitatory postsynaptic current; MSSN, striatal medium-sized spiny neuron; PPF, paired-pulse facilitation; PPR, paired-pulse ratio; TTX, tetrodotoxin.

References

- Aizman, O., Brismar, H., Uhlen, P., Zettergren, E., Levey, A.I., Forssberg, H., Greengard, P. & Aperia, A. (2000) Anatomical and physiological evidence for D1 and D2 dopamine receptor colocalization in neostriatal neurons. *Nat. Neurosci.*, **3**, 226–230.
- Albin, R.L., Reiner, A., Anderson, K.D., Dure, L.S. 4th, Handelin, B., Balfour, R., Whetsell, W.O. Jr, Penney, J.B. & Young, A.B. (1992) Preferential loss of striato-external pallidal projection neurons in presymptomatic Huntington's disease. *Ann. Neurol.*, **31**, 425–430.
- Alzheimer, C., Schwindt, P.C. & Crill, W.E. (1993) Postnatal development of a persistent Na⁺ current in pyramidal neurons from rat sensorimotor cortex. *J. Neurophysiol.*, **69**, 290–292.
- Bargas, J., Howe, A., Eberwine, J., Cao, Y. & Surmeier, D.J. (1994) Cellular and molecular characterization of Ca²⁺ currents in acutely isolated, adult rat neostriatal neurons. *J. Neurosci.*, **14**, 6667–6686.
- Bernard, V., Normand, E. & Bloch, B. (1992) Phenotypical characterization of the rat striatal neurons expressing muscarinic receptor genes. *J. Neurosci.*, **12**, 3591–3600.
- Berretta, S., Parthasarathy, H.B. & Graybiel, A.M. (1997) Local release of GABAergic inhibition in the motor cortex induces immediate-early gene expression in indirect pathway neurons of the striatum. *J. Neurosci.*, **17**, 4752–4763.
- Bracci, E., Centonze, D., Bernardi, G. & Calabresi, P. (2004) Engagement of rat striatal neurons by cortical epileptiform activity investigated with paired recordings. *J. Neurophysiol.*, **92**, 2725–2737.
- Brorson, J.R., Li, D. & Suzuki, T. (2004) Selective expression of heteromeric AMPA receptors driven by flip-flop differences. *J. Neurosci.*, **24**, 3461–3470.
- Burnashev, N., Khodorova, A., Jonas, P., Helm, P.J., Wisden, W., Monyer, H., Seeburg, P.H. & Sakmann, B. (1992) Calcium-permeable AMPA-kainate receptors in fusiform cerebellar glial cells. *Science*, **256**, 1566–1570.
- Calabresi, P., Mercuri, N.B., Sancesario, G. & Bernardi, G. (1993) Electrophysiology of dopamine-denervated striatal neurons. Implications for Parkinson's disease. *Brain*, **116**, 433–452.
- Cepeda, C., Walsh, J.P., Hull, C.D., Howard, S.G., Buchwald, N.A. & Levine, M.S. (1989) Dye-coupling in the neostriatum of the rat. I. Modulation by dopamine-depleting lesions. *Synapse*, **4**, 229–237.
- Cepeda, C., Walsh, J.P., Peacock, W., Buchwald, N.A. & Levine, M.S. (1994) Neurophysiological, pharmacological and morphological properties of human caudate neurons recorded in vitro. *Neuroscience*, **59**, 89–103.
- Cepeda, C., Colwell, C.S., Itri, J.N., Chandler, S.H. & Levine, M.S. (1998) Dopaminergic modulation of NMDA-induced whole cell currents in neostriatal neurons in slices: contribution of calcium conductances. *J. Neurophysiol.*, **79**, 82–94.
- Cepeda, C., Hurst, R.S., Altemus, K.L., Flores-Hernandez, J., Calvert, C.R., Jokel, E.S., Grandy, D.K., Low, M.J., Rubinstein, M., Ariano, M.A. & Levine, M.S. (2001) Facilitated glutamatergic transmission in the striatum of D2 dopamine receptor-deficient mice. *J. Neurophysiol.*, **85**, 659–670.
- Cepeda, C., Hurst, R.S., Calvert, C.R., Hernandez-Echeagaray, E., Nguyen, O.K., Jocoy, E., Christian, L.J., Ariano, M.A. & Levine, M.S. (2003) Transient and progressive electrophysiological alterations in the corticostriatal pathway in a mouse model of Huntington's disease. *J. Neurosci.*, **23**, 961–969.
- Cepeda, C., Starling, A.J., Wu, N., Soda, T., Lobo, M.K., Yang, X.W. & Levine, M.S. (2004) Defining electrophysiological properties of subpopulations of striatal neurons using genetic expression of enhanced green fluorescent protein. *Soc. Neurosci. Abstr.*, **30**, 307.4.
- Cepeda, C., Wu, N., André, V.M., Cummings, D.M. & Levine, M.S. (2007) The corticostriatal pathway in Huntington's disease. *Prog. Neurobiol.*, **81**, 253–271.
- Day, M., Wang, Z., Ding, J., An, X., Ingham, C.A., Shering, A.F., Wokosin, D., Ilijic, E., Sun, Z., Sampson, A.R., Mugnaini, E., Deutch, A.Y., Sesack, S.R., Arbuthnot, G.W. & Surmeier, D.J. (2006) Selective elimination of

- glutamatergic synapses on striatopallidal neurons in Parkinson disease models. *Nat. Neurosci.*, **9**, 251–259.
- Deng, Y.P., Albin, R.L., Penney, J.B., Young, A.B., Anderson, K.D. & Reiner, A. (2004) Differential loss of striatal projection systems in Huntington's disease: a quantitative immunohistochemical study. *J. Chem. Neuroanat.*, **27**, 143–164.
- Deng, Y.P., Xie, J.P., Wang, H.B., Lei, W.L., Chen, Q. & Reiner, A. (2007) Differential localization of the GluR1 and GluR2 subunits of the AMPA-type glutamate receptor among striatal neuron types in rats. *J. Chem. Neuroanat.*, **33**, 167–192.
- Florio, T., Di Loreto, S., Cerrito, F. & Scarnati, E. (1993) Influence of prefrontal and sensorimotor cortices on striatal neurons in the rat: electrophysiological evidence for converging inputs and the effects of 6-OHDA-induced degeneration of the substantia nigra. *Brain Res.*, **619**, 180–188.
- Fusco, F.R., Chen, Q., Lamoreaux, W.J., Figueredo-Cardenas, G., Jiao, Y., Coffman, J.A., Surmeier, D.J., Honig, M.G., Carlock, L.R. & Reiner, A. (1999) Cellular localization of huntingtin in striatal and cortical neurons in rats: lack of correlation with neuronal vulnerability in Huntington's disease. *J. Neurosci.*, **19**, 1189–1202.
- Galarraga, E., Bargas, J., Martinez-Fong, D. & Aceves, J. (1987) Spontaneous synaptic potentials in dopamine-denervated neostriatal neurons. *Neurosci. Lett.*, **81**, 351–355.
- Geiger, J.R., Melcher, T., Koh, D.S., Sakmann, B., Seeburg, P.H., Jonas, P. & Monyer, H. (1995) Relative abundance of subunit mRNAs determines gating and Ca²⁺ permeability of AMPA receptors in principal neurons and interneurons in rat CNS. *Neuron*, **15**, 193–204.
- Gerfen, C.R. (1992) The neostriatal mosaic: multiple levels of compartmental organization. *Trends Neurosci.*, **15**, 133–139.
- Gong, S., Zheng, C., Doughty, M.L., Losos, K., Didkovsky, N., Schambra, U.B., Nowak, N.J., Joyner, A., Leblanc, G., Hatten, M.E. & Heintz, N. (2003) A gene expression atlas of the central nervous system based on bacterial artificial chromosomes. *Nature*, **425**, 917–925.
- Gubellini, P., Picconi, B., Bari, M., Battista, N., Calabresi, P., Centonze, D., Bernardi, G., Finazzi-Agro, A. & Maccarrone, M. (2002) Experimental parkinsonism alters endocannabinoid degradation: implications for striatal glutamatergic transmission. *J. Neurosci.*, **22**, 6900–6907.
- Gutnick, M.J., Connors, B.W. & Prince, D.A. (1982) Mechanisms of neocortical epileptogenesis in vitro. *J. Neurophysiol.*, **48**, 1321–1335.
- Kawaguchi, Y., Wilson, C.J. & Emson, P.C. (1989) Intracellular recording of identified neostriatal patch and matrix spiny cells in a slice preparation preserving cortical inputs. *J. Neurophysiol.*, **62**, 1052–1068.
- Kawaguchi, Y., Wilson, C.J. & Emson, P.C. (1990) Projection subtypes of rat neostriatal matrix cells revealed by intracellular injection of biocytin. *J. Neurosci.*, **10**, 3421–3438.
- Kemp, J.M. & Powell, T.P. (1971) The structure of the caudate nucleus of the cat: light and electron microscopy. *Philos. Trans. R. Soc. Lond. B Biol. Sci.*, **262**, 383–401.
- Kreitzer, A.C. & Malenka, R.C. (2007) Endocannabinoid-mediated rescue of striatal LTD and motor deficits in Parkinson's disease models. *Nature*, **445**, 643–647.
- Lei, W., Jiao, Y., Del Mar, N. & Reiner, A. (2004) Evidence for differential cortical input to direct pathway versus indirect pathway striatal projection neurons in rats. *J. Neurosci.*, **24**, 8289–8299.
- Levesque, M. & Parent, A. (2005) The striatofugal fiber system in primates: a reevaluation of its organization based on single-axon tracing studies. *Proc. Natl Acad. Sci. U.S.A.*, **102**, 11 888–11 893.
- Mallet, N., Ballion, B., Le Moine, C. & Gonon, F. (2006) Cortical inputs and GABA interneurons imbalance projection neurons in the striatum of parkinsonian rats. *J. Neurosci.*, **26**, 3875–3884.
- Menalled, L., Zanjani, H., MacKenzie, L., Koppel, A., Carpenter, E., Zeitlin, S. & Chesselet, M.F. (2000) Decrease in striatal enkephalin mRNA in mouse models of Huntington's disease. *Exp. Neurol.*, **162**, 328–342.
- Mink, J.W. (1996) The basal ganglia: focused selection and inhibition of competing motor programs. *Prog. Neurobiol.*, **50**, 381–425.
- Morishima, M. & Kawaguchi, Y. (2006) Recurrent connection patterns of corticostriatal pyramidal cells in frontal cortex. *J. Neurosci.*, **26**, 4394–4405.
- Partin, K.M., Fleck, M.W. & Mayer, M.L. (1996) AMPA receptor flip/flop mutants affecting deactivation, desensitization, and modulation by cyclothiazide, aniracetam, and thiocyanate. *J. Neurosci.*, **16**, 6634–6647.
- Reiner, A., Albin, R.L., Anderson, K.D., D'Amato, C.J., Penney, J.B. & Young, A.B. (1988) Differential loss of striatal projection neurons in Huntington disease. *Proc. Natl Acad. Sci. U.S.A.*, **85**, 5733–5737.
- Sapp, E., Ge, P., Aizawa, H., Bird, E., Penney, J., Young, A.B., Vonsattel, J.P. & DiFiglia, M. (1995) Evidence for a preferential loss of enkephalin immunoreactivity in the external globus pallidus in low grade Huntington's disease using high resolution image analysis. *Neuroscience*, **64**, 397–404.
- Sara, Y., Virmani, T., Deák, F., Liu, X. & Kavalali, E.T. (2005) An isolated pool of vesicles recycles at rest and drives spontaneous neurotransmission. *Neuron*, **45**, 563–573.
- Saviane, C., Savtchenko, L.P., Raffaelli, G., Voronin, L.L. & Cherubini, E. (2002) Frequency-dependent shift from paired-pulse facilitation to paired-pulse depression at unitary CA3-CA3 synapses in the rat hippocampus. *J. Physiol.*, **544**, 469–476.
- Shen, W., Tian, X., Day, M., Ulrich, S., Tkatch, T., Nathanson, N.M. & Surmeier, D.J. (2007) Cholinergic modulation of Kir2 channels selectively elevates dendritic excitability in striatopallidal neurons. *Nat. Neurosci.*, Sept. 30; Epub ahead of print.
- Smith, Y., Bevan, M.D., Shink, E. & Bolam, J.P. (1998) Microcircuitry of the direct and indirect pathways of the basal ganglia. *Neuroscience*, **86**, 353–387.
- Smith, R., Musleh, W., Akopian, G., Buckwalter, G. & Walsh, J.P. (2001) Regional differences in the expression of corticostriatal synaptic plasticity. *Neuroscience*, **106**, 95–101.
- Surmeier, D.J., Song, W.J. & Yan, Z. (1996) Coordinated expression of dopamine receptors in neostriatal medium spiny neurons. *J. Neurosci.*, **16**, 6579–6591.
- Tallaksen-Greene, S.J. & Albin, R.L. (1996) Splice variants of glutamate receptor subunits 2 and 3 in striatal projection neurons. *Neuroscience*, **75**, 1057–1064.
- Tseng, K.Y., Kasanetz, F., Kargieman, L., Riquelme, L.A. & Murer, M.G. (2001) Cortical slow oscillatory activity is reflected in the membrane potential and spike trains of striatal neurons in rats with chronic nigrostriatal lesions. *J. Neurosci.*, **21**, 6430–6439.
- Uryu, K., Butler, A.K. & Chesselet, M.F. (1999) Synaptogenesis and ultrastructural localization of the polysialylated neural cell adhesion molecule in the developing striatum. *J. Comp. Neurol.*, **405**, 216–232.
- Venance, L. & Glowinski, J. (2003) Heterogeneity of spike frequency adaptation among medium spiny neurones from the rat striatum. *Neuroscience*, **122**, 77–92.
- Vorobjev, V.S., Sharonova, I.N., Haas, H.L. & Sergeeva, O.A. (2000) Differential modulation of AMPA receptors by cyclothiazide in two types of striatal neurons. *Eur. J. Neurosci.*, **12**, 2871–2880.